NeuroImage: Clinical 25 (2020) 102153

Contents lists available at ScienceDirect

NeuroImage: Clinical

journal homepage: www.elsevier.com/locate/ynicl

Protein-based amide proton transfer-weighted MR imaging of amnestic mild cognitive impairment

Zewen Zhang[a,b], Caiqing Zhang[c], Jian Yao[a], Xin Chen[a], Fei Gao[a], Shanshan Jiang[b], Weibo Chen[d], Jinyuan Zhou[b], Guangbin Wang[a,*]

[a] Department of MR, Shandong Medical Imaging Research Institute, Shandong University, Jinan, Shandong, China
[b] Division of MR Research, Department of Radiology, Johns Hopkins University, MD, United States
[c] Department of Respiratory Medicine, Shandong Provincial Qianfoshan Hospital, Shandong University, Jinan, Shandong, China
[d] Philips Healthcare, Shanghai, China

ARTICLE INFO

Keywords:
Alzheimer's disease
Mild cognitive impairment
Magnetic resonance imaging
Molecular imaging
Biomarkers

ABSTRACT

Amide proton transfer-weighted (APTw) MRI is a novel molecular imaging technique that can noninvasively detect endogenous cellular proteins and peptides in tissue. Here, we demonstrate the feasibility of protein-based APTw MRI in characterizing amnestic mild cognitive impairment (aMCI). Eighteen patients with confirmed aMCI and 18 matched normal controls were scanned at 3 Tesla. The APTw, as well as conventional magnetization transfer ratio (MTR), signal differences between aMCI and normal groups were assessed by the independent samples *t*-test, and the receiver-operator-characteristic analysis was used to assess the diagnostic performance of APTw. When comparing the normal control group, aMCI brains typically had relatively higher APTw signals. Quantitatively, APTw intensity values were significantly higher in nine of 12 regions of interest in aMCI patients than in normal controls. The largest areas under the receiver-operator-characteristic curves were 0.88 (gray matter in occipital lobe) and 0.82 (gray matter in temporal lobe, white matter in occipital lobe) in diagnosing aMCI patients. On the contrary, MTR intensity values were significantly higher in only three of 12 regions of interest in the aMCI group. Additionally, the age dependency analyses revealed that these cross-sectional APTw/MTR signals had an increasing trend with age in most brain regions for normal controls, but a decreasing trend with age in most brain regions for aMCI patients. Our early results show the potential of the APTw signal as a new imaging biomarker for the noninvasive molecular diagnosis of aMCI.

1. Introduction

With the world population aging, the incidence of dementia, especially the most common form, Alzheimer's disease (AD), is estimated to increase markedly, which will cause enormous health and economic crises. Unfortunately, there are only symptomatic treatments at present. Much previous research has demonstrated that the pathologic processes of AD precede the first symptoms of cognitive decline (Mattsson et al., 2009). Some elderly patients who have cognitively declined, but who do not meet the diagnostic criteria for AD, are often known to have mild cognitive impairment (MCI) (Albert et al., 2011; Petersen, 2004; Petersen et al., 1999), which generally represents a prodromal phase of AD. Over 50 percent of these MCI individuals progress to AD within five years (Gauthier et al., 2006). It is now widely believed that the Aβ proteins and the tau proteins can synergistically promote the progression of normal neurons to AD as their accumulation into plaques and tangles (Bloom, 2014). Furthermore, MCI can be classified into amnestic (aMCI) and non-amnestic subtypes (naMCI) with different structures (Csukly et al., 2016). Compared to the naMCI subtype, the aMCI subtype has a higher conversion rate to AD (Grundman et al., 2004), whereas the naMCI subtype is prone to progress to other dementia subtypes, such as vascular dementia (Gyebnar et al., 2018). Currently, it is fully recognized (Jack et al., 2018) that the continued development of new unrecognized biomarkers that can reliably diagnose MCI patients and predict their conversion to AD (Da et al., 2014; Misra et al., 2009; Nir et al., 2013; Ottoy et al., 2019; Young et al.,

Abbreviations: AD, Alzheimer's disease; aMCI, amnestic mild cognitive impairment; APTw, amide proton transfer-weighted; CEST, chemical exchange saturation transfer; MMSE, mini mental state examination; MRI, magnetic resonance imaging; MTR, magnetization transfer ratio; ROC, receiver-operator-characteristic; ROI, region of interest

* Corresponding author.
E-mail address: wgb7932596@hotmail.com (G. Wang).

https://doi.org/10.1016/j.nicl.2019.102153
Received 23 September 2019; Received in revised form 7 December 2019; Accepted 26 December 2019
Available online 27 December 2019

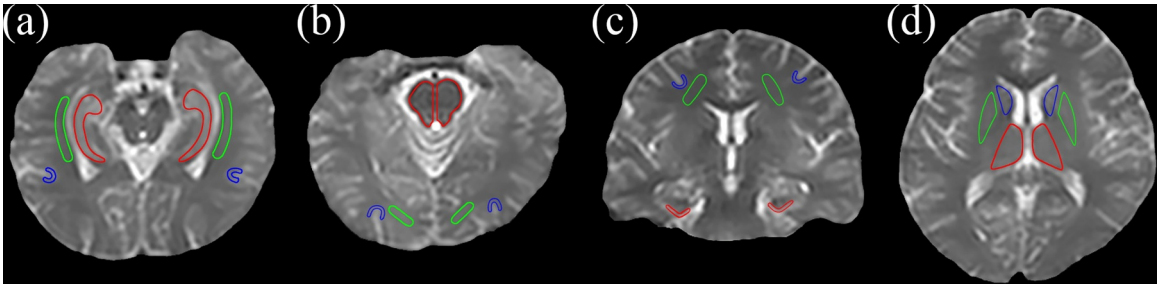

Fig. 1. An example of the 12 regions of interest (ROIs) for quantitative analyses. (**a**) The first slice: hippocampus (red), the white matter in the temporal lobe (green), and the gray matter in the temporal lobe (blue); (**b**) the second slice: pons (red), the white matter in the occipital lobe (green), and the gray matter in the occipital lobe (blue); (**c**) the third slice: the entorhinal cortex (red), the white matter in the frontal lobe (green), and the gray matter in the frontal lobe (blue); and (**d**) the fourth slice: the thalamus (red), the putamen (green), and the caudate nucleus (blue). (For interpretation of the references to colour in this figure legend, the reader is referred to the web version of this article.)

2013; Zhang et al., 2011) are deeply needed, which makes early intervention possible and may greatly improve the prognosis for AD patients.

Amide proton transfer-weighted (APTw) MRI, a specific type of chemical exchange saturation transfer (CEST) imaging (Jones et al., 2018; Kogan et al., 2013; Ward et al., 2000; Zhou and Van Zijl, 2006), is a promising molecular imaging technique that can noninvasively detect cellular endogenous mobile proteins and peptides (Zhou et al., 2019). Since first reported in 2003 (Zhou et al., 2003a, b), APT imaging has been researched as an imaging biomarker for several diseases, ranging from brain tumors (Choi et al., 2017; Jiang et al., 2019, 2017; Togao et al., 2017) to other non-oncologic neurologic diseases, such as stroke (Harston et al., 2014; Heo et al., 2017b), Parkinson's disease (Li et al., 2014), and traumatic brain injury (Zhang et al., 2017a). Notably, recent work has shown that the APTw values of the bilateral hippocampus were significantly higher in AD patients than in normal controls (Wang et al., 2015). However, whether APTw MRI can be an effective diagnostic method for MCI is still unknown. This proof-of-concept study aimed to assess the potential of using the APTw signal as a new imaging biomarker for the differentiation of patients with aMCI and healthy controls, with a comparison with conventional magnetization transfer (MT) imaging that is quantified by the MR ratio (MTR) associated with semi-solid macromolecules in tissue (Henkelman et al., 2001).

2. Material and methods

2.1. Subjects

The local institutional review board approved this study, and all subjects gave written, informed consent. Inclusion criteria for the study were as follows: ≥40 years old; diagnosed as aMCI by an experienced neurodegenerative-disease specialist according to the criteria described by Petersen (2004) and Petersen et al. (1999) and the National Institute of Aging and Alzheimer's Association recommendations (Albert et al., 2011); no history of head trauma, central nervous system infection, or cerebral structural lesions; or no psychiatric diseases and exposure to psychotropic drugs.

2.2. MRI protocol

MR imaging was performed on a 3 Tesla MRI scanner (Achieva; Philips Medical Systems). For the aMCI patients, scanning was implemented immediately after the diagnoses. A single-slice, multi-offset, combined APTw and conventional MT imaging acquisition protocol (Li et al., 2014) was applied to the maximum cross-sectional areas of the hippocampus, the pons, the entorhinal cortex, and the thalamus (four slices). The APTw sequence parameters were as follows: block pulse radiofrequency saturation duration = 800 ms; saturation power = 2 μT; repetition time = 3000 ms; field of view = 230 × 220 mm^2; matrix = 105 × 100 (reconstructed to be 256 × 256); slice thickness = 6 mm; and turbo spin-echo factor = 54. The 32 offsets were, respectively, 0, ± 0.25, ± 0.5, ± 0.75, ± 1, ± 1.5, ± 2 (2), ± 2.5 (2), ± 3 (2), ± 3.25 (2), ± 3.5 (6), ± 3.75 (2), ± 4 (2), ± 4.5, ± 5, ± 6, and +15.6 ppm (the numbers in brackets indicate the number of acquisitions, which was 1 unless specified). The acquisition time of this combined scan was about 12 min (3 min each slice).

2.3. Data analysis

The Interactive Data Language (IDL, version 8; Exelis Visual Information Solutions, Inc.) was applied for image analysis. Briefly, the measured MT spectra were corrected for B_0 field inhomogeneity effects on a voxel-by-voxel basis, as described previously (Wen et al., 2010). As usual, the semi-solid MTR images were constructed by 1 - M_{sat}(+15.6 ppm)/M_0 (in which M_{sat} and M_0 indicate, respectively, the imaging signal intensities with and without selective radiofrequency irradiation). The APTw images were constructed by the MTR asymmetry (MTR_{asym}) at the offsets of ± 3.5 ppm, namely, MTR_{asym}(3.5 ppm) = M_{sat} (−3.5 ppm)/M_0 - M_{sat} (+3.5 ppm)/M_0 (Zhou et al., 2003a, b).

Based on the structural M_{sat}(3.5 ppm) and M_0 images co-registered with APTw for each subject, 12 regions of interest (ROIs) were manually drawn by two radiologists (Z.Z. and G.W., who have had five and 30 years of experience in neurological imaging, respectively). These 12 ROIs were as follows (Fig. 1): the hippocampus, the white matter in the temporal lobe and the gray matter in the temporal lobe (the first slice); the pons, the white matter in the occipital lobe and the gray matter in the occipital lobe (the second slice); the entorhinal cortex, the white matter in the frontal lobe and the gray matter in the frontal lobe (the third slice); and the thalamus, putamen and caudate nucleus (the fourth slice). For each subject, the mean MTR value, mean APTw value, and APTw histogram data of both hemispheres were reported.

2.4. Statistical analysis

All data were analyzed by the statistical software SPSS (version 25.0; IBM Corporation). After a test of normality, the chi-square test and independent samples *t*-test were applied to analyze the statistical differences in the demographic, clinical, and quantitative imaging parameters between aMCI patients and normal controls. The receiver-operator-characteristic (ROC) analysis was used to assess the diagnostic performance of APTw values at each ROI. Furthermore, the correlation analysis was performed for the APTw/MTR signals and age. A $P < 0.05$ was deemed statistically significant.

Table 1
Population statistics for normal and aMCI groups.

Parameter	Normal people (n = 18)	aMCI Patients (n = 18)	P Value
Group age (y)	56.2 ± 8.9 (40–75)	62.1 ± 10.3 (40–80)	0.074
Age of men (y)	54.6 ± 8.0 (40–65)	60.3 ± 12.2 (40–80)	0.266
Age of women (y)	57.9 ± 9.9 (44–75)	63.6 ± 8.9 (44–76)	0.202
Percentage of women	50	56	0.747
MMSE	28.4 ± 1.1 (27–30)	25.3 ± 0.8 (24–26)	<0.0001

Data are means ± standard deviations, with ranges in parentheses; aMCI, amnestic mild cognitive impairment; MMSE, mini-mental state examination.

3. Results

3.1. Patient demographics

From December 2017 to October 2018, 18 aMCI patients who met the inclusion criteria and 18 matched normal controls were enrolled and participated in scanning. The descriptive information for these two groups is provided in Table 1. There was no difference in age or sex ratio ($P > 0.05$).

3.2. Comparison of APTw images for normal controls and aMCI patients

The two examples of MTR and APTw images for the normal controls and for the aMCI patients are shown in Fig. 2. Compared to the normal controls, the APTw images of the aMCI patients demonstrated visible, relatively higher APTw signals in most brain regions, corresponding to right-shifted APTw histograms (Fig. 3). There were no clearly visual differences between the MTR images of the normal and aMCI groups.

3.3. Quantitative analyses for APTw and MTR data

Fig. 4 summarizes differences between ROI-based mean APTw signal intensity values for the normal controls and aMCI patients, based on the independent samples t-test. There were significantly higher APTw values in nine of 12 ROIs in aMCI patients than in normal controls: the hippocampus ($P = 0.0407$), the white matter in the temporal lobe ($P = 0.0027$), the gray matter in the temporal lobe ($P = 0.0155$), the pons ($P = 0.0279$), the white matter in the occipital lobe ($P = 0.0008$), the gray matter in the occipital lobe ($P = 0.0011$), the white matter in the frontal lobe ($P = 0.0012$), the thalamus ($P = 0.0199$), and the putamen ($P = 0.0062$). In three remaining ROIs (the entorhinal cortex, the gray matter in the frontal lobe, and the caudate nucleus), the APTw values in the aMCI group showed a trend toward higher levels, but the increases were not statistically significant, compared to the normal control group ($P > 0.05$).

Differences between ROI-based mean MTR values for the two groups are indicated in Fig. 5. The average MTR values of aMCI patients were slightly larger than those of normal controls in almost all ROIs (except for the gray matter in the temporal lobe). However, these MTR values showed significant differences in only three ROIs: the pons ($P = 0.0409$), the thalamus ($P = 0.0080$), and the caudate nucleus ($P = 0.0386$).

3.4. Accuracy of APTw MRI in diagnosing aMCI

For nine ROIs showing significantly higher APTw values in aMCI patients than in normal controls, the ROC curve analysis (Fig. 6) showed that APTw MRI had great potential as a new imaging biomarker for the diagnosis of aMCI patients. The largest areas under the ROC curves (Table 2) were 0.88 in the gray matter in the occipital lobe (with an 88.9% sensitivity and a 72.2% specificity at the cutoff APTw signal intensity of −0.47%), and 0.82 in the gray matter in the temporal lobe (with an 88.9% sensitivity and a 77.8% specificity at the cutoff APTw signal intensity of −0.26%) and the white matter in the occipital lobe (with an 83.3% sensitivity and a 72.2% specificity at the cutoff APTw signal intensity of −0.76%) for the noninvasive molecular diagnosis of aMCI.

3.5. Age dependencies of cross-sectional APTw/MTR signals

Additional correlation analyses of the APTw and MTR signals of different ages were performed for the two groups (Table 3 and Supporting Figs. S1–S4). In the normal control group, the APTw values showed significant positive correlations with age in four of 12 ROIs analyzed: the white matter in the temporal lobe ($r = 0.5869$, $P = 0.0104$), the gray matter in the temporal lobe ($r = 0.5954$, $P = 0.0091$), the white matter in the occipital lobe ($r = 0.7007$, $P = 0.0012$), and the white matter in the frontal lobe ($r = 0.4731$, $P = 0.0474$). In almost all remaining ROIs (except for the caudate nucleus), the APTw values indicated a statistically insignificant, increasing trend with age ($r > 0$, $P > 0.05$). Furthermore, the MTR values of seven of 12 ROIs (the hippocampus, the white matter in the temporal lobe, the pons, the white matter in the occipital lobe, the gray matter in the occipital lobe, the thalamus, and the caudate nucleus) showed an increasing trend with age ($r > 0$, $P > 0.05$).

In the aMCI group, the APTw values of eight ROIs (the hippocampus, the gray matter in the temporal lobe, the pons, the white matter in the occipital lobe, the gray matter in the occipital lobe, the white matter in the frontal lobe, the gray matter in the frontal lobe, the thalamus) revealed a trend toward decreasing levels with age ($r < 0$, $P > 0.05$). Moreover, the MTR values of almost all ROIs (except for the thalamus and caudate nucleus) displayed a trend toward decreasing levels with age ($r < 0$, $P > 0.05$).

4. Discussion

In this study, we have demonstrated the feasibility and value of using the APTw MRI signal as a new imaging biomarker for the diagnosis of aMCI that represents a prodromal phase of AD. It was found that the mean APTw values were significantly higher in 9/12 ROIs in the aMCI patients than those in the normal controls (Fig. 4). On the contrary, the MTR values revealed significant differences in only 3/12 ROIs between the normal and aMCI groups (Fig. 5). Interestingly, the age dependency analyses showed that these cross-sectional APTw/MTR signals were seemingly age dependent in both groups (Table 3). Conventional MT imaging quantified by MTR is designed to detect semi-solid macromolecules that exist in the solid environment of cells, for instance, proteins in the cell membrane and the nucleus (Henkelman et al., 2001), while APT imaging is sensitive to mobile proteins in tissues (Zhou et al., 2019). These mobile proteins have a specific amide proton resonance frequency at 3.5 ppm downfield from water, which can be detected by APTw MRI. Theoretically, the larger the concentration of amide protons, the higher the APTw value would be.

A hallmark of neurodegenerative proteinopathies is the accumulation of misfolded proteins in the brain (Sweeney et al., 2017; Wyss-Coray, 2016). According to the amyloid hypothesis, which is currently the predominant theory for the cause of AD (Hardy and Higgins, 1992; Selkoe, 1991), abnormal accumulation of amyloid beta (Aβ) protein in the brain is the main effect of AD pathogenesis, and tau protein tangle deposition and neurodegeneration are regarded as downstream influences of an imbalance between production and clearance of Aβ protein (Hardy and Selkoe, 2002). In addition, the amyloid deposition begins in the basal frontal and temporal lobes while the neurofibrillary tangle deposition starts in the medial temporal lobe, and gradually both of the abnormal proteins spread throughout the entire cerebral cortex (Petrella, 2013). Therefore, the ability to image underlying Aβ protein plaques and tau protein neurofibrillary tangles *in vivo* represents a

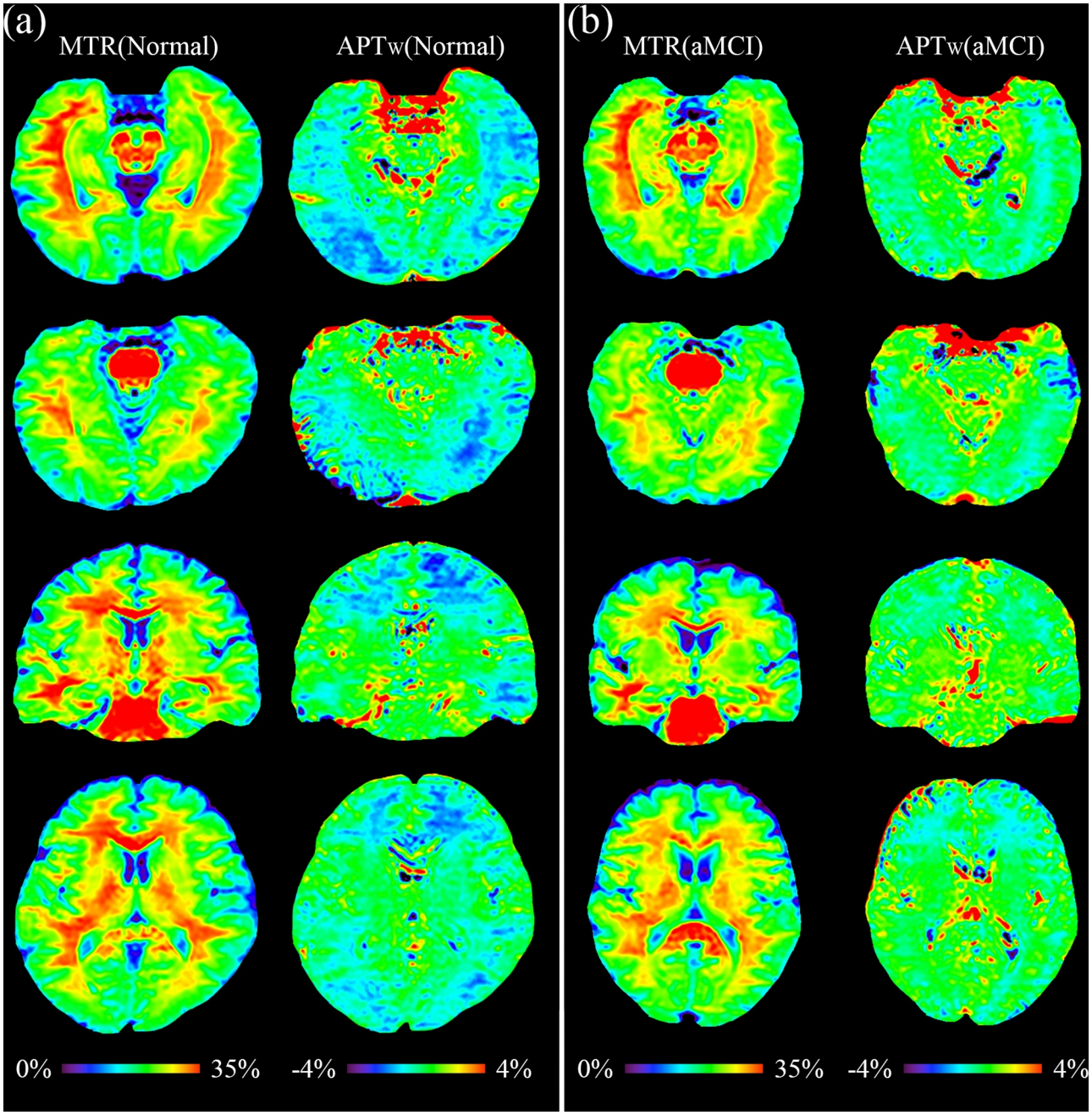

Fig. 2. MTR images and APTw images for (**a**) a normal adult (male; 46 y) and (**b**) aMCI patient (female; 61 y).

major area of progress for AD research (Petrella, 2013). Currently, PET has been able to accurately target Aβ protein (Seibyl et al., 2011; Yang et al., 2012) and tau protein (Shoghi-Jadid et al., 2002; Small et al., 2006) in the brain using relevant tracers. The accumulation, aggregation, and eventual insolubility of various proteins, including amyloid beta and tau protein, might provide an observable MT imaging effect (Perez-Torres et al., 2014; Ridha et al., 2007). This molecular mechanism may also account for the APTw results reported in this study; thus, APTw imaging can be a potential means by which to noninvasively visualize the abnormal proteins of aMCI patients *in vivo*.

Further, the APTw values showed significant differences between the two groups in more ROIs than the MTR values. The APTw values in nine ROIs were significantly higher in the aMCI group than in the normal control group, suggesting that the abnormal proteins had accumulated in the corresponding nine areas of aMCI patients. The entorhinal cortex, the earliest area invaded by tau proteins (Petrella, 2013), and the most heavily damaged cortex in Alzheimer's disease (Van Hoesen et al., 1991), should have had the higher APTw value in the aMCI group. However, the APTw value of the entorhinal cortex did not show significant differences between the two groups. The reason may be attributable to the following: the abnormal protein deposition gradually causes damage and the death of entorhinal cortex neurons (Bloom, 2014). At a certain stage, the neuronal death may cause the mobile protein loss, as observed in the substantia nigra in Parkinson's disease (Li et al., 2014). The exact mechanism needs to be explored in the future.

In the normal control group, both the APTw and MTR values showed weak positive correlations or trends toward increasing levels with age in most brain regions (11 of 12 ROIs for APTw, and 7 of 12 ROIs for MTR) (Table 3). It is known that there is no significant neuronal loss during aging in normal brains (Martínez-Pinilla et al., 2016), and cerebral volume loss with advancing age is attributed to changes in

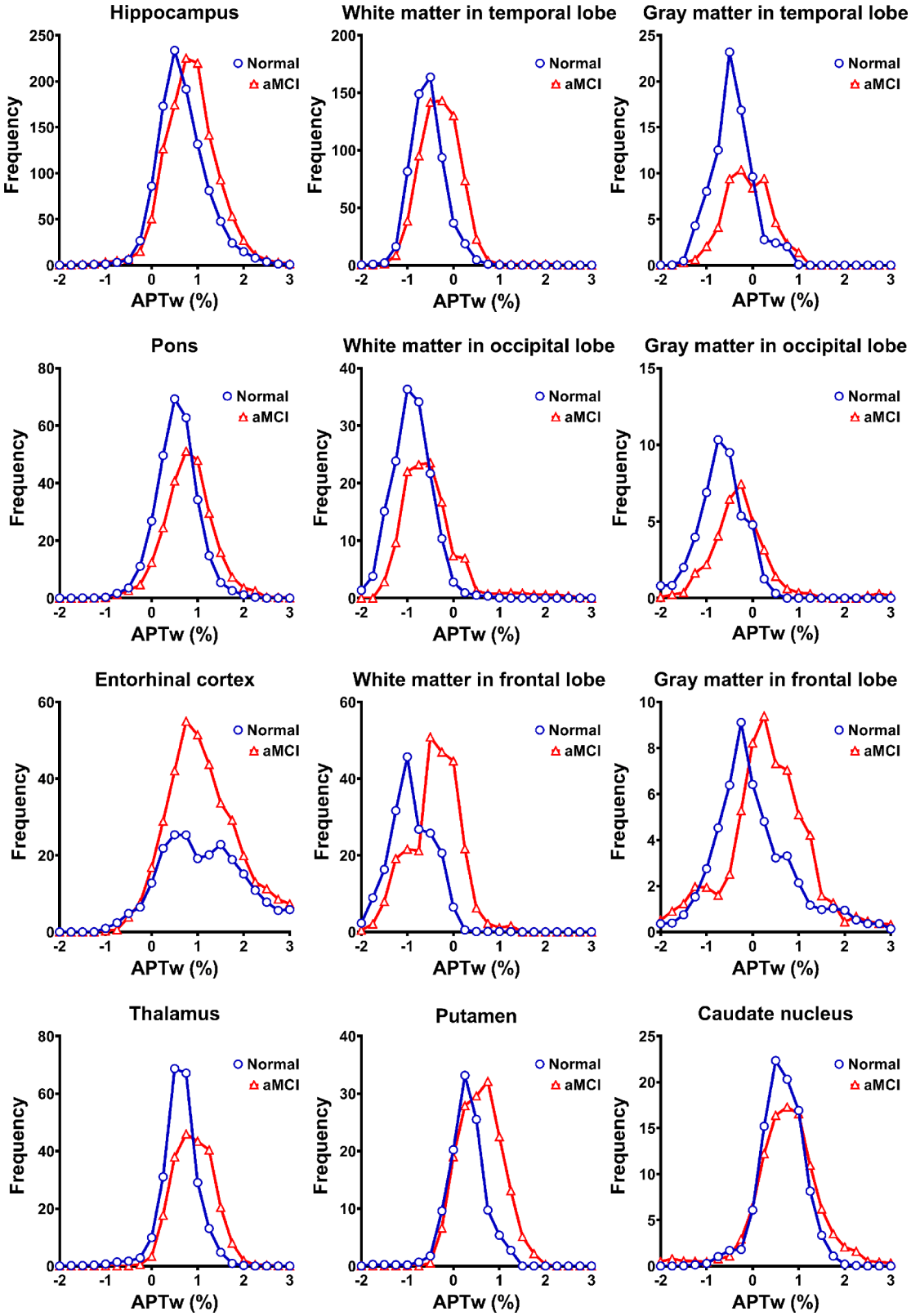

Fig. 3. The average APTw histograms acquired from 12 regions of interest (ROIs) of normal (blue) and aMCI (red) groups. The histograms of aMCI patients were slightly right-shifted compared to those of normal controls in all ROIs (except for the entorhinal cortex). (For interpretation of the references to colour in this figure legend, the reader is referred to the web version of this article.)

neuronal size and dendritic arborization (Thulborn et al., 2016). Thus, the concentration of mobile proteins and semi-solid macromolecules in cerebral tissue may become relatively higher with increasing age, which may explain the positive correlations in the normal control group. On the contrary, in the aMCI group, both the APTw and MTR values showed a trend toward decreasing levels with age for most brain regions (8/12 ROIs for APTw, and 10/12 ROIs for MTR) (Table 3). The loss of neurons in aMCI is induced by Aβ and tau protein deposition

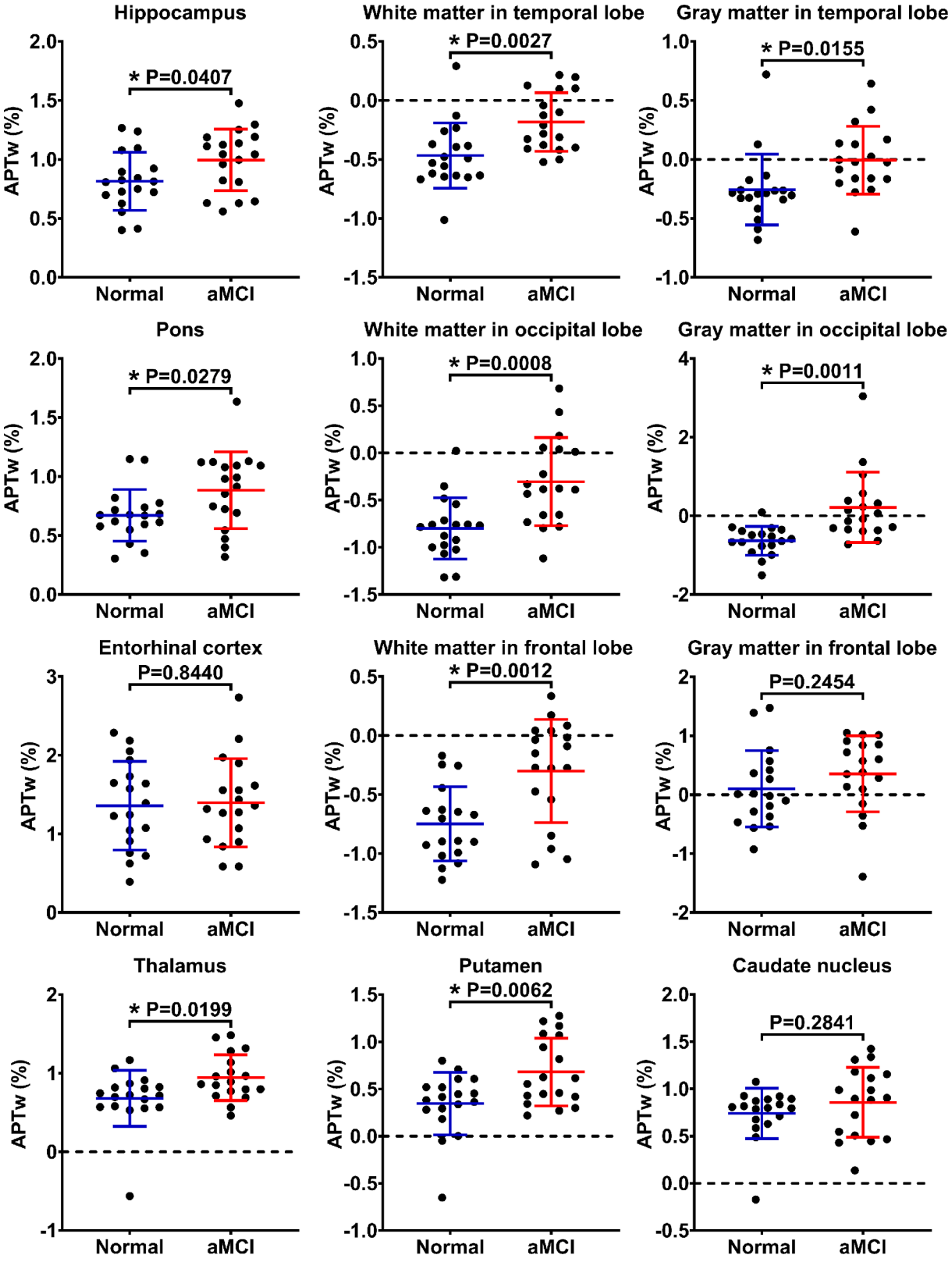

Fig. 4. The independent samples *t*-test for the APTw values. The results are shown from the 12 regions of interest (ROIs) in the normal (blue) and aMCI (red) groups. *$P < 0.05$. (For interpretation of the references to colour in this figure legend, the reader is referred to the web version of this article.)

(Bloom, 2014). Therefore, we inferred that more neurons in the cerebrum of aMCI patients are lost with advancing age, which may represent a greater possibility of conversion to AD. From the above analysis, we deduced that the higher, decreasing APTw and MTR values in aMCI patients and the lower, increasing APTw and MTR values in normal controls would converge at a certain point with aging. After the convergence point, the APTw and MTR values in aMCI patients may be equal to or even lower than those in normal controls, consistent with a

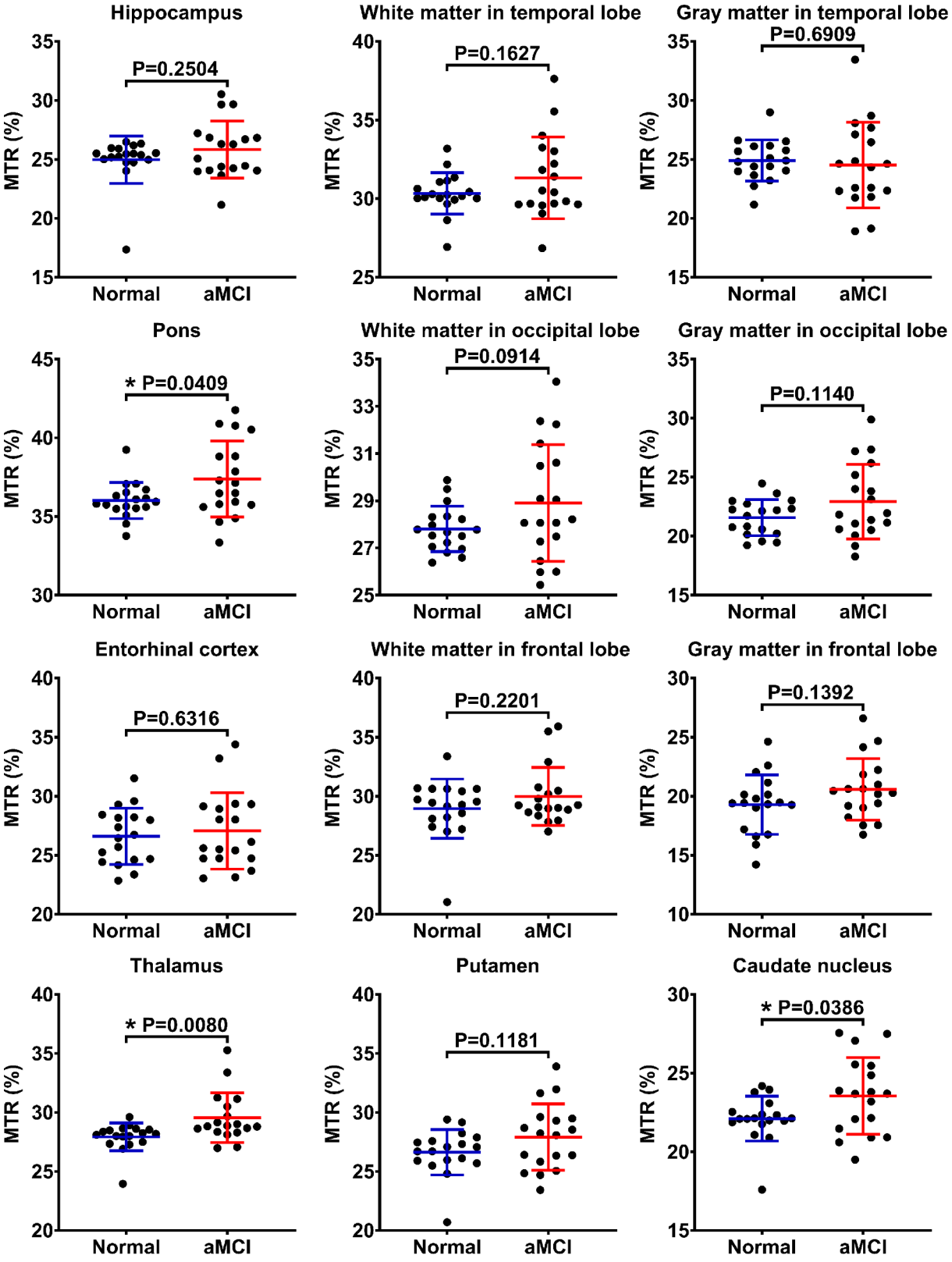

Fig. 5. The independent samples *t*-test for the MTR values. The results are shown from the 12 regions of interest (ROIs) in the normal (blue) and aMCI (red) groups. *$P < 0.05$. (For interpretation of the references to colour in this figure legend, the reader is referred to the web version of this article.)

previous report for relatively older subjects (Mascalchi et al., 2013).

There were some limitations to this study. (i) The number of participants was relatively small in this study. We are planning to perform a further longitudinal study with a larger number of participants. A regression-based analysis approach adjusted for age, mini-mental state examination (MMSE), educational attainment, and any other potential influential factors will be performed in the future. (ii) We acquired four cerebral slices using a single-slice protocol. Thus, the MRI signals in

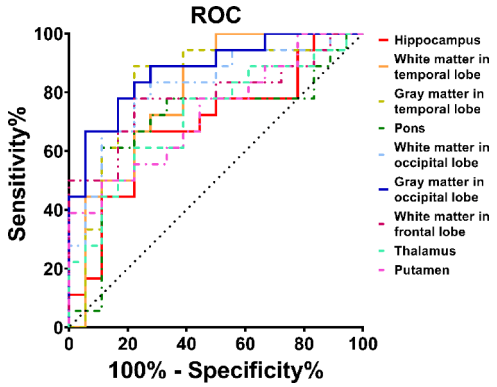

Fig. 6. Receiver-operator-characteristic (ROC) analysis of APTw imaging intensities as an imaging biomarker for the diagnosis of aMCI.

other regions of brain could not be explored in the study. In the future, we plan to increase the coverage of APTw MRI by applying a three-dimensional APT imaging acquisition protocol that has been reported in the literature (Zhou et al., 2013), with which the APTw MRI of the whole brain can be obtained. Further, because of the limited slice, ROI placement was manually performed, which was difficult for cortical grey matters. The three-dimensional APT imaging acquisition protocol in combination with the automatic segmentation may increase the ROI accuracy in the future. (iii) We hypothesize that the abnormal accumulation and aggregation of various proteins, including amyloid beta and tau protein, provided the observed APT imaging effect. It was reported that soluble amyloid beta and tau protein in the AD brain had levels of a few to tens of μM (Han et al., 2017; McDonald et al., 2012). In this regard, it should be kept in mind that the observed APTw MRI signal is associated with a large group of cellular proteins, each contributing multiple amide groups, as shown in a previous proteomics study (Yan et al., 2015). (iv) The APTw signal quantified from MTR_{asym}(3.5 ppm), as used in this study, was contaminated with the upfield nuclear Overhauser enhancement signal from mobile and semi-solid protons (Jones et al., 2013; Ling et al., 2008), and several possible other effects (Zhou et al., 2019). An alternative APTw imaging analysis or acquisition approach (Heo et al., 2016a, b; Xu et al., 2016; Zaiss et al., 2011; Zhang et al., 2017b; Zu et al., 2013) may be used to quantify a pure APT effect in the future studies. A higher MTR (Fig. 5) or a lower T_1 (Tang et al., 2018) may potentially decrease the corresponding APTw signal. Notably, it has been shown recently that the mixing APTw image contrast is dominated by the APT effect (Heo et al., 2016a, b) and the possible influence of water T_1 on APTw imaging was actually small for the pulse sequence parameters used here (Heo et al., 2017a; Zu, 2018). Crucially, the use of MR fingerprinting may achieve absolute APT parameter quantification for exchange rates and concentrations (Cohen et al., 2018; Heo et al., 2019; Zhou et al., 2018). It is expected that more pure and quantitative APT MRI approaches have significance for improving the detection accuracy, but this still will have to be validated.

5. Conclusion

This exploratory study represents the first analysis of the ability to use APTw MRI to detect patients with aMCI. The significant APTw signal differences in the multiple ROIs between aMCI patients and normal controls demonstrated the feasibility of APTw MRI to be used for the noninvasive molecular diagnosis of aMCI, which could make possible early intervention for aMCI, and even AD. Thus, our early results highlight the future potential of the APTw signal as an imaging biomarker for aMCI patients.

Informed consent

Informed consent was obtained from all individual participants included in the study.

CRediT authorship contribution statement

Zewen Zhang: Conceptualization, Formal analysis, Investigation, Methodology, Software, Visualization, Writing - original draft, Writing - review & editing. **Caiqing Zhang:** Data curation, Investigation, Resources, Writing - original draft, Writing - review & editing. **Jian Yao:** Formal analysis, Validation, Software, Writing - review & editing. **Xin Chen:** Data curation, Validation, Writing - review & editing. **Fei Gao:** Data curation, Validation, Writing - review & editing. **Shanshan Jiang:** Formal analysis, Visualization, Writing - review & editing. **Weibo Chen:** Methodology, Software, Visualization, Writing - review & editing. **Jinyuan Zhou:** Formal analysis, Visualization, Writing - review & editing. **Guangbin Wang:** Conceptualization, Methodology, Project administration, Supervision, Software, Writing - review & editing.

Declaration of Competing Interests

Dr. Jinyuan Zhou is a co-inventor on a patent for the APT MRI technology. This patent is owned and managed by Johns Hopkins University. Other authors declare that they have no conflicts of interest.

Acknowledgments

The authors thank Ms. Mary McAllister for editorial assistance.

Table 2
Diagnostic performance of APTw signals from nine regions of interest (ROIs) in predicting aMCI.

ROIs	AUC (95% CI)	Sensitivity (95% CI) (%)	Specificity (95% CI) (%)	PPV (95% CI) (%)	NPV (95% CI) (%)	Cutoff Value (%)
Hippocampus	0.70 (0.51–0.83)	66.7 (41.0–86.7)	77.8 (52.4–93.6)	75.0 (54.4–88.3)	70.0 (53.7–82.4)	0.92
White matter in temporal lobe	0.80 (0.63–0.91)	100.0 (81.5–100.0)	50.0 (26.0–74.0)	66.7 (55.8–76.0)	100.0	−0.53
Gray matter in temporal lobe	0.82 (0.66–0.93)	88.9 (65.3–98.6)	77.8 (52.4–93.6)	80.0 (62.4–90.6)	87.5 (64.9–96.4)	−0.26
Pons	0.70 (0.52–0.84)	61.1 (35.7–82.7)	88.9 (65.3–98.6)	84.6 (58.6–95.5)	69.6 (55.6–80.7)	0.82
White matter in occipital lobe	0.82 (0.65–0.93)	83.3 (58.6–96.4)	72.2 (46.5–90.3)	75.0 (58.1–86.7)	81.2 (59.7–92.7)	−0.76
Gray matter in occipital lobe	0.88 (0.72–0.96)	88.9 (65.3–98.6)	72.2 (46.5–90.3)	76.2 (59.9–87.3)	86.7 (63.0–96.1)	−0.47
White matter in frontal lobe	0.78 (0.62–0.90)	77.8 (52.4–93.6)	77.8 (52.4–93.6)	77.8 (58.8–89.6)	77.8 (58.8–89.6)	−0.63
Thalamus	0.72 (0.54–0.85)	77.8 (52.4–93.6)	61.1 (35.7–82.7)	66.7 (51.6–79.0)	73.3 (51.8–87.6)	0.75
Putamen	0.73 (0.56–0.86)	50.0 (26.0–74.0)	88.9 (65.3–98.6)	81.8 (53.0–94.7)	64.0 (52.1–74.4)	0.61

APTw, amide proton transfer-weighted; aMCI, amnestic mild cognitive; AUC, area under the ROC (receiver operator characteristic) curve; CI, confidence interval; PPV, positive predictive value; NPV, negative predictive value.

Table 3
Correlation results between the APTw/MTR signals and age from 12 regions of interest (ROIs) of normal and aMCI groups.

	Normal controls				Patients with aMCI			
	APTw		**MTR**		**APTw**		**MTR**	
	r	***P***	***r***	***P***	***r***	***P***	***r***	***P***
Hippocampus	0.3971	0.1028	0.1229	0.6271	−0.0336	0.8948	−0.4168	0.0853
White matter in temporal lobe	**0.5869**	**0.0104**	0.3153	0.2025	0.2666	0.2848	−0.3391	0.1687
Gray matter in temporal lobe	**0.5954**	**0.0091**	−0.1885	0.4538	−0.0765	0.7630	−0.3293	0.1821
Pons	0.4017	0.0984	0.3664	0.1348	−0.2674	0.2834	−0.1574	0.5327
White matter in occipital lobe	**0.7007**	**0.0012**	0.3797	0.1202	−0.0364	0.8859	−0.1359	0.5909
Gray matter in occipital lobe	0.3501	0.1544	0.2995	0.2272	−0.0908	0.7201	−0.3207	0.1944
Entorhinal cortex	0.2586	0.3002	−0.2108	0.4011	0.2723	0.2743	−0.3221	0.1924
White matter in frontal lobe	**0.4731**	**0.0474**	−0.0283	0.9114	−0.2729	0.2733	−0.1470	0.5605
Gray matter in frontal lobe	0.1642	0.5150	−0.0985	0.6975	−0.1469	0.5608	−0.2124	0.3975
Thalamus	0.0425	0.8671	0.0653	0.7969	−0.1083	0.6688	0.0020	0.9937
Putamen	0.1187	0.6391	−0.0011	0.9964	0.1538	0.5423	−0.2329	0.3524
Caudate nucleus	−0.1367	0.5887	0.0721	0.7762	0.0537	0.8325	0.1096	0.6652

APTw, amide proton transfer-weighted; MTR, magnetization transfer ratio; aMCI, amnestic mild cognitive impairment. Bold values mean $P < 0.05$.

Supplementary materials

Supplementary material associated with this article can be found, in the online version, at doi:10.1016/j.nicl.2019.102153.

References

Albert, M.S., DeKosky, S.T., Dickson, D., Dubois, B., Feldman, H.H., Fox, N.C., Gamst, A., Holtzman, D.M., Jagust, W.J., Petersen, R.C., Snyder, P.J., Carrillo, M.C., Thies, B., Phelps, C.H., 2011. The diagnosis of mild cognitive impairment due to Alzheimer's disease: recommendations from the National Institute on Aging-Alzheimer's Association workgroups on diagnostic guidelines for Alzheimer's disease. Alzheimer's Dementia 7, 270–279.

Bloom, G.S., 2014. Amyloid-β and tau: the trigger and bullet in Alzheimer disease pathogenesis. JAMA Neurol. 71, 505–508.

Choi, Y.S., Ahn, S.S., Lee, S.K., Chang, J.H., Kang, S.G., Kim, S.H., Zhou, J., 2017. Amide proton transfer imaging to discriminate between low- and high-grade gliomas: added value to apparent diffusion coefficient and relative cerebral blood volume. Eur. Radiol. 27, 3181–3189.

Cohen, O., Huang, S., McMahon, M.T., Rosen, M.S., Farrar, C.T., 2018. Rapid and quantitative chemical exchange saturation transfer (CEST) imaging with magnetic resonance fingerprinting (MRF). Magn. Reson. Med. 80, 2449–2463.

Csukly, G., Siraly, E., Fodor, Z., Horvath, A., Salacz, P., Hidasi, Z., Csibri, E., Rudas, G., Szabo, A., 2016. The differentiation of amnestic type MCI from the non-amnestic types by structural MRI. Front. Aging Neurosci. 8, 52.

Da, X., Toledo, J.B., Zee, J., Wolk, D.A., Xie, S.X., Ou, Y.M., Shacklett, A., Parmpi, P., Shaw, L., Trojanowski, J.Q., Davatzikos, C., 2014. Integration and relative value of biomarkers for prediction of MCI to AD progression: spatial patterns of brain atrophy, cognitive scores, APOE genotype and CSF biomarkers. NeuroImage Clin. 4, 164–173.

Gauthier, S., Reisberg, B., Zaudig, M., Petersen, R.C., Ritchie, K., Broich, K., Belleville, S., Brodaty, H., Bennett, D., Chertkow, H., Cummings, J.L., de Leon, M., Feldman, H., Ganguli, M., Hampel, H., Scheltens, P., Tierney, M.C., Whitehouse, P., Winblad, B., 2006. Mild cognitive impairment. Lancet 367, 1262–1270.

Grundman, M., Petersen, R., Ferris, S., Thomas, R.G., Aisen, P.S., Bennett, D.A., Foster, N.L., Jack Jr., C.R., Galasko, D.R., Doody, R., 2004. Mild cognitive impairment can be distinguished from Alzheimer disease and normal aging for clinical trials. Arch. Neurol. 61, 59–66.

Gyebnar, G., Szabo, A., Siraly, E., Fodor, Z., Sákovics, A., Salacz, P., Hidasi, Z., Csibri, E., Rudas, G., Kozak, L.R., 2018. What can DTI tell about early cognitive impairment?–Differentiation between MCI subtypes and healthy controls by diffusion tensor imaging. Psych. Res. 272, 46–57.

Han, P., Serrano, G., Beach, T.G., Caselli, R.J., Yin, J., Zhuang, N., Shi, J., 2017. A quantitative analysis of brain soluble tau and the tau secretion factor. J. Neuropathol. Exp. Neurol. 76, 44–51.

Hardy, J., Selkoe, D.J., 2002. The amyloid hypothesis of Alzheimer's disease: progress and problems on the road to therapeutics. Science 297, 353–356.

Hardy, J.A., Higgins, G.A., 1992. Alzheimer's disease: the amyloid cascade hypothesis. Science 256, 184–185.

Harston, G.W.J., Tee, Y.-K., Blockley, N., Okell, T.W., Thandeswaran, S., Shaya, G., Sheerin, F., Cellerini, M., Payne, S., Jezzard, P., 2014. Identifying the ischaemic penumbra using pH-weighted magnetic resonance imaging. Brain 138, 36–42.

Henkelman, R.M., Stanisz, G.J., Graham, S.J., 2001. Magnetization transfer in MRI: a review. NMR Biomed. 14, 57–64.

Heo, H.-Y., Zhang, Y., Lee, D.-H., Hong, X., Zhou, J., 2016a. Quantitative assessment of amide proton transfer (APT) and nuclear Overhauser enhancement (NOE) imaging with extrapolated semi-solid magnetization transfer reference (EMR) signals: application to a rat glioma model at 4.7 T. Magn. Reson. Med. 75, 137–138.

Heo, H.Y., Han, Z., Jiang, S., Schar, M., van Zijl, P.C.M., Zhou, J., 2019. Quantifying amide proton exchange rate and concentration in chemical exchange saturation transfer imaging of the human brain. Neuroimage 189, 202–213.

Heo, H.Y., Lee, D.H., Zhang, Y., Zhao, X., Jiang, S., Chen, M., Zhou, J., 2017a. Insight into the quantitative metrics of chemical exchange saturation transfer (CEST) imaging. Magn. Reson. Med. 77, 1853–1865.

Heo, H.Y., Zhang, Y., Burton, T.M., Jiang, S., Zhao, Y., van Zijl, P.C.M., Leigh, R., Zhou, J., 2017b. Improving the detection sensitivity of pH-weighted amide proton transfer MRI in acute stroke patients using extrapolated semisolid magnetization transfer reference signals. Magn. Reson. Med. 78, 871–880.

Heo, H.Y., Zhang, Y., Jiang, S., Lee, D.H., Zhou, J., 2016b. Quantitative assessment of amide proton transfer (APT) and nuclear overhauser enhancement (NOE) imaging with extrapolated semisolid magnetization transfer reference (EMR) signals: II. Comparison of three EMR models and application to human brain glioma at 3 Tesla. Magn. Reson. Med. 75, 1630–1639.

Jack Jr., C.R., Bennett, D.A., Blennow, K., Carrillo, M.C., Dunn, B., Haeberlein, S.B., Holtzman, D.M., Jagust, W., Jessen, F., Karlawish, J., Liu, E., Molinuevo, J.L., Montine, T., Phelps, C., Rankin, K.P., Rowe, C.C., Scheltens, P., Siemers, E., Snyder, H.M., Sperling, R., 2018. NIA-AA research framework: toward a biological definition of Alzheimer's disease. Alzheimer's Dementia 14, 535–562.

Jiang, S., Eberhart, C.G., Lim, M., Heo, H.-Y., Zhang, Y., Blair, L., Wen, Z., Holdhoff, M., Lin, D., Huang, P., Qin, H., Quinones-Hinojosa, A., Weingart, J.D., Barker, P.B., Pomper, M.G., Laterra, J., van Zijl, P.C.M., Blakeley, J.O., Zhou, J., 2019. Identifying recurrent malignant glioma after treatment using amide proton transfer-weighted MR imaging: a validation study with image-guided stereotactic biopsy. Clin. Cancer Res. 25, 552–561.

Jiang, S., Zou, T., Eberhart, C.G., Villalobos, M.A., Heo, H.Y., Zhang, Y., Wang, Y., Wang, X., Yu, H., Du, Y., 2017. Predicting IDH mutation status in grade II gliomas using amide proton transfer-weighted (APTw) MRI. Magn. Reson. Med. 78, 1100–1109.

Jones, C.K., Huang, A., Xu, J., Edden, R.A., Schar, M., Hua, J., Oskolkov, N., Zaca, D., Zhou, J., McMahon, M.T., Pillai, J.J., van Zijl, P.C., 2013. Nuclear Overhauser enhancement (NOE) imaging in the human brain at 7T. Neuroimage 77, 114–124.

Jones, K.M., Pollard, A.C., Pagel, M.D., 2018. Clinical applications of chemical exchange saturation transfer (CEST) MRI. J. Magn. Reson. Imaging 47, 11–27.

Kogan, F., Hariharan, H., Reddy, R., 2013. Chemical exchange saturation transfer (CEST) imaging: description of technique and potential clinical applications. Curr. Radiol. Rep. 1, 102–114.

Li, C., Peng, S., Wang, R., Chen, H., Su, W., Zhao, X., Zhou, J., Chen, M., 2014. Chemical exchange saturation transfer MR imaging of Parkinson's disease at 3 Tesla. Eur. Radiol. 24, 2631–2639.

Ling, W., Regatte, R.R., Navon, G., Jerschow, A., 2008. Assessment of glycosaminoglycan concentration *in vivo* by chemical exchange-dependent saturation transfer (gagCEST). Proc. Natl. Acad. Sci. (USA) 105, 2266–2270.

Martínez-Pinilla, E., Ordonez, C., del Valle, E., Navarro, A., Tolivia, J., 2016. Regional and gender study of neuronal density in brain during aging and in alzheimer's disease. Front. Aging Neuros. 8, 213.

Mascalchi, M., Ginestroni, A., Bessi, V., Toschi, N., Padiglioni, S., Ciulli, S., Tessa, C., Giannelli, M., Bracco, L., Diciotti, S., 2013. Regional analysis of the magnetization transfer ratio of the brain in mild Alzheimer disease and amnestic mild cognitive impairment. AJNR Am. J. Neurorad. 34, 2098–2104.

Mattsson, N., Zetterberg, H., Hansson, O., Andreasen, N., Parnetti, L., Jonsson, M., Herukka, S.-K., van der Flier, W.M., Blankenstein, M.A., Ewers, M., 2009. CSF biomarkers and incipient Alzheimer disease in patients with mild cognitive impairment. JAMA 302, 385–393.

McDonald, J.M., Cairns, N.J., Taylor-Reinwald, L., Holtzman, D., Walsh, D.M., 2012. The levels of water-soluble and triton-soluble Abeta are increased in Alzheimer's disease brain. Brain Res. 1450, 138–147.

Misra, C., Fan, Y., Davatzikos, C., 2009. Baseline and longitudinal patterns of brain atrophy in MCI patients, and their use in prediction of short-term conversion to AD: results from ADNI. Neuroimage 44, 1415–1422.
Nir, T.M., Jahanshad, N., Villalon-Reina, J.E., Toga, A.W., Jack, C.R., Weiner, M.W., Thompson, P.M., 2013. Effectiveness of regional DTI measures in distinguishing Alzheimer's disease, MCI, and normal aging. NeuroImage Clin. 3, 180–195.
Ottoy, J., Niemantsverdriet, E., Verhaeghe, J., De Roeck, E., Struyfs, H., Somers, C., Wyffels, L., Ceyssens, S., Van Mossevelde, S., Van den Bossche, T., Van Broeckhoven, C., Ribbens, A., Bjerke, M., Stroobants, S., Engelborghs, S., Staelens, S., 2019. Association of short-term cognitive decline and MCI-to-AD dementia conversion with CSF, MRI, amyloid- and F-18-FDG-PET imaging. NeuroImage Clin. 22. https://doi.org/10.1016/j.nicl.2019.101771.
Perez-Torres, C.J., Reynolds, J.O., Pautler, R.G., 2014. Use of magnetization transfer contrast MRI to detect early molecular pathology in Alzheimer's disease. Magn. Reson. Med. 71, 333–338.
Petersen, R.C., 2004. Mild cognitive impairment as a diagnostic entity. J. Intern. Med. 256, 183–194.
Petersen, R.C., Smith, G.E., Waring, S.C., Ivnik, R.J., Tangalos, E.G., Kokmen, E., 1999. Mild cognitive impairment: clinical characterization and outcome. Arch. Neurol. 56, 303–308.
Petrella, J.R., 2013. Neuroimaging and the search for a cure for Alzheimer disease. Radiology 269, 671–691.
Ridha, B.H., Symms, M.R., Tozer, D.J., Stockton, K.C., Frost, C., Siddique, M.M., Lewis, E.B., MacManus, D.G., Boulby, P.A., Barker, G.J., Rossor, M.N., Fox, N.C., Tofts, P.S., 2007. Magnetization transfer ratio in Alzheimer disease: comparison with volumetric measurements. AJNR Am. J. Neuroradiol. 28, 965–970.
Seibyl, J., Zubal, I.G., Jennings, D., Marek, K., Doraiswamy, P.M., 2011. Molecular PET imaging in multicenter Alzheimer's therapeutic trials: current trends and implementation strategies. Expert Rev. Neurotherap. 11, 1783–1793.
Selkoe, D.J., 1991. The molecular pathology of Alzheimer's disease. Neuron 6, 487–498.
Shoghi-Jadid, K., Small, G.W., Agdeppa, E.D., Kepe, V., Ercoli, L.M., Siddarth, P., Read, S., Satyamurthy, N., Petric, A., Huang, S.-.C., 2002. Localization of neurofibrillary tangles and beta-amyloid plaques in the brains of living patients with Alzheimer disease. Am. J. Geriatr. Psych. 10, 24–35.
Small, G.W., Kepe, V., Ercoli, L.M., Siddarth, P., Bookheimer, S.Y., Miller, K.J., Lavretsky, H., Burggren, A.C., Cole, G.M., Vinters, H.V., 2006. PET of brain amyloid and tau in mild cognitive impairment. New Engl. J. Med. 355, 2652–2663.
Sweeney, P., Park, H., Baumann, M., Dunlop, J., Frydman, J., Kopito, R., McCampbell, A., Leblanc, G., Venkateswaran, A., Nurmi, A., Hodgson, R., 2017. Protein misfolding in neurodegenerative diseases: implications and strategies. Transl. Neurodegener. 6, 6.
Tang, X., Cai, F., Ding, D.X., Zhang, L.L., Cai, X.Y., Fang, Q., 2018. Magnetic resonance imaging relaxation time in Alzheimer's disease. Brain Res. Bull. 140, 176–189.
Thulborn, K., Lui, E., Guntin, J., Jamil, S., Sun, Z., Claiborne, T.C., Atkinson, I.C., 2016. Quantitative sodium MRI of the human brain at 9.4 T provides assessment of tissue sodium concentration and cell volume fraction during normal aging. NMR Biomed. 29, 137–143.
Togao, O., Hiwatashi, A., Yamashita, K., Kikuchi, K., Keupp, J., Yoshimoto, K., Kuga, D., Yoneyama, M., Suzuki, S.O., Iwaki, T., Takahashi, M., Iihara, K., Honda, H., 2017. Grading diffuse gliomas without intense contrast enhancement by amide proton transfer MR imaging: comparisons with diffusion- and perfusion-weighted imaging. Eur. Radiol. 27, 578–588.
Van Hoesen, G.W., Hyman, B.T., Damasio, A.R., 1991. Entorhinal cortex pathology in Alzheimer's disease. Hippocampus 1, 1–8.
Wang, R., Li, S.-.Y., Chen, M., Zhou, J.-.Y., Peng, D.-.T., Zhang, C., Dai, Y.-.M., 2015. Amide proton transfer magnetic resonance imaging of Alzheimer's disease at 3.0 Tesla: a preliminary study. Chin. Med. J. 128, 615.
Ward, K.M., Aletras, A.H., Balaban, R.S., 2000. A new class of contrast agents for MRI based on proton chemical exchange dependent saturation transfer (CEST). J. Magn. Reson. 143, 79–87.
Wen, Z., Hu, S., Huang, F., Wang, X., Guo, L., Quan, X., Wang, S., Zhou, J., 2010. MR imaging of high-grade brain tumors using endogenous protein and peptide-based contrast. Neuroimage 51, 616–622.
Wyss-Coray, T., 2016. Ageing, neurodegeneration and brain rejuvenation. Nature 539, 180–186.
Xu, X., Yadav, N.N., Zeng, H., Jones, C.K., Zhou, J., van Zijl, P.C., Xu, J., 2016. Magnetization transfer contrast-suppressed imaging of amide proton transfer and relayed nuclear overhauser enhancement chemical exchange saturation transfer effects in the human brain at 7T. Magn. Reson. Med. 75, 88–96.
Yan, K., Fu, Z., Yang, C., Zhang, K., Jiang, S., Lee, D.-.H., Heo, H.-.Y., Zhang, Y., Cole, R.N., Van Eyk, J.E., 2015. Assessing amide proton transfer (APT) MRI contrast origins in 9L gliosarcoma in the rat brain using proteomic analysis. Mol. Imag. Biol. 17, 479–487.
Yang, L., Rieves, D., Ganley, C., 2012. Brain amyloid imaging—FDA approval of florbetapir F18 injection. New Engl. J. Med. 367, 885–887.
Young, J., Modat, M., Cardoso, M.J., Mendelson, A., Cash, D., Ourselin, S., 2013. Accurate multimodal probabilistic prediction of conversion to Alzheimer's disease in patients with mild cognitive impairment. NeuroImage Clin. 2, 735–745.
Zaiss, M., Schmitt, B., Bachert, P., 2011. Quantitative separation of CEST effect from magnetization transfer and spillover effects by Lorentzian-line-fit analysis of z-spectra. J. Magn. Reson. 211, 149–155.
Zhang, D., Wang, Y., Zhou, L., Yuan, H., Shen, D., 2011. Multimodal classification of Alzheimer's disease and mild cognitive impairment. Neuroimage 55, 856–867.
Zhang, H., Wang, W., Jiang, S., Zhang, Y., Heo, H.Y., Wang, X., Peng, Y., Wang, J., Zhou, J., 2017a. Amide proton transfer-weighted MRI detection of traumatic brain injury in rats. J. Cereb. Blood Flow Metab. 37, 3422–3432.
Zhang, X.Y., Wang, F., Li, H., Xu, J., Gochberg, D.F., Gore, J.C., Zu, Z., 2017b. Accuracy in the quantification of chemical exchange saturation transfer (CEST) and relayed nuclear Overhauser enhancement (rNOE) saturation transfer effects. NMR Biomed. 30, e3716.
Zhou, J., Heo, H.-Y., Knutsson, L., van Zijl, P.C.M., Jiang, S., 2019. APT-weighted MRI: techniques, current neuro applications, and challenging issues. J. Magn. Reson. Imaging. https://doi.org/10.1002/jmri.26645.
Zhou, J., Lal, B., Wilson, D.A., Laterra, J., Van Zijl, P.C., 2003a. Amide proton transfer (APT) contrast for imaging of brain tumors. Magn. Reson. Med. 50, 1120–1126.
Zhou, J., Payen, J.-.F., Wilson, D.A., Traystman, R.J., Van Zijl, P.C., 2003b. Using the amide proton signals of intracellular proteins and peptides to detect pH effects in MRI. Nat. Med. 9, 1085.
Zhou, J., Van Zijl, P.C., 2006. Chemical exchange saturation transfer imaging and spectroscopy. Progr. Nucl. Magn. Reson. Spectr. 48, 109–136.
Zhou, J., Zhu, H., Lim, M., Blair, L., Quinones-Hinojosa, A., Messina, S.A., Eberhart, C.G., Pomper, M.G., Laterra, J., Barker, P.B., 2013. Three-dimensional amide proton transfer MR imaging of gliomas: initial experience and comparison with gadolinium enhancement. J. Magn. Reson. Imaging 38, 1119–1128.
Zhou, Z., Han, P., Zhou, B., Christodoulou, A.G., Shaw, J.L., Deng, Z., Li, D., 2018. Chemical exchange saturation transfer fingerprinting for exchange rate quantification. Magn. Reson. Med. 80, 1352–1363.
Zu, Z., Janve, V.A., Xu, J., Does, M.D., Gore, J.C., Gochberg, D.F., 2013. A new method for detecting exchanging amide protons using chemical exchange rotation transfer. Magn. Reson. Med. 69, 637–647.
Zu, Z.L., 2018. Towards the complex dependence of MTRasym on T-1w in amide proton transfer (APT) imaging. NMR Biomed. 31. https://doi.org/10.1002/nbm.3934.